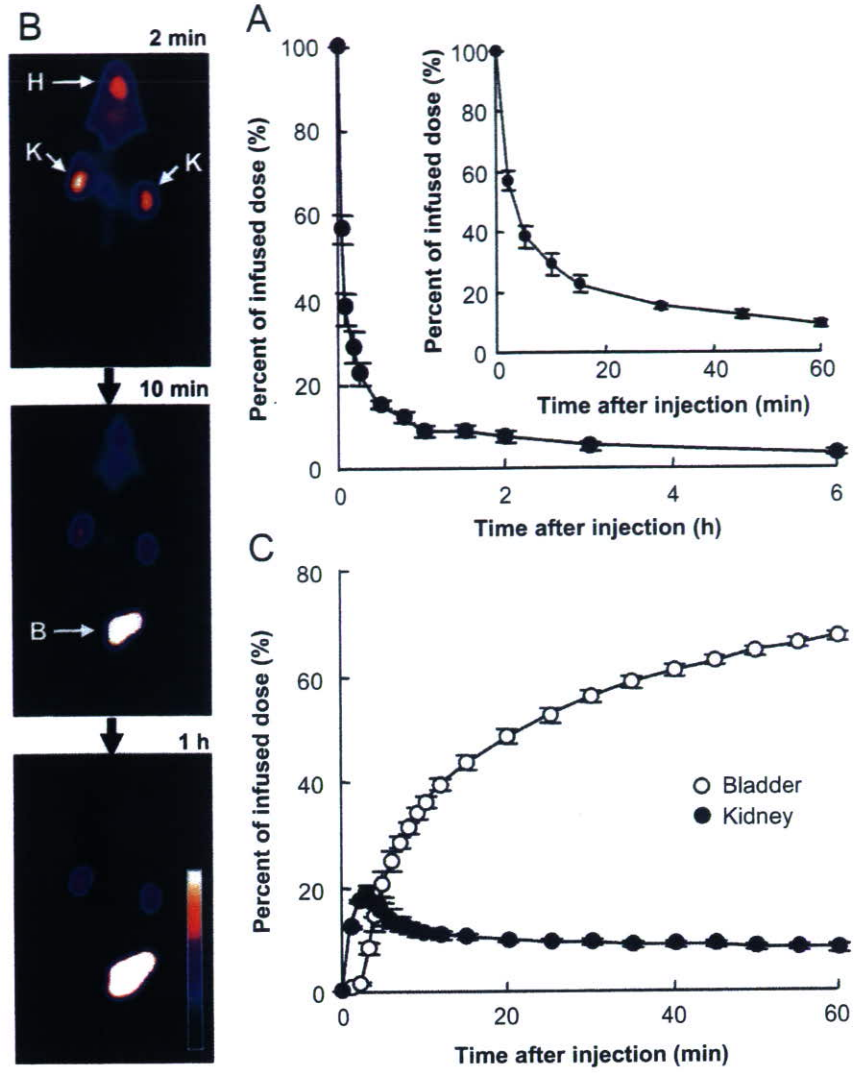

Fig. 2. Circulation and distribution kinetics of mixture of ^{99m}Tc-HMPAO and glutathione without encapsulation in vesicles after i.v. infusion in rabbits. (A) Circulation kinetics (B) Gamma camera images of rabbits acquired at various times after infusion. H: heart, K: kidney, B: bladder. (C) Distribution profiles as a percentage of the injected dose analyzed from the gamma camera images.

describing the relationship of 12 times that of a femur as being equivalent to whole bone in rabbits [28].

3.4. Microscopic localization of PEG(0.6)-[SA-Ve] in bone marrow

The initial studies were designed to demonstrate that PEG(0.6)-[SA-Ve] functions as a nanoparticulate carrier as well as identify their microscopic localization in tissues. We used PEG(0.6)-[SA-Ve] double-labeled by encapsulating water-soluble TR-SOD in an aqueous phase and embedding lipid-soluble C_1-BODIPY C_{12} in bilayer membrane (Fig. 5(A)). As shown in Fig. 5(B), the bone marrow sections have fluorescence from both the TR-SOD and C_1-BODIPY C_{12}. The fluorescence was locally concentrated, and larger fluorescent domain was 30 μm in size along the long axis. Fluorescent distribution in red pulp of spleen was dense, whereas it was sparse in liver. An important finding from this observation is that the fluorescence from membrane probes and encapsulated probes are co-localized in bone marrow. These images clearly indicate that PEG(0.6)-[SA-Ve] functions as a nanoparticle-carrier to deliver the encapsulated agents to bone marrow tissues. A second study was performed to identify the histological location of PEG(0.6)-[SA-Ve] in bone marrow. Femoral bone marrow tissue was taken from rabbit at 6 h after i.v. injection of PEG(0.6)-[SA-Ve] and examined using TEM. TEM observation clearly demonstrated the location of PEG(0.6)-[SA-Ve] in bone marrow (Figs. 6(A) and (B)). A massive number of vesicles were trapped in endosomes and lysosomes of BMMϕ, but no vesicles were observed in cytoplasm and cell nucleus (Fig. 6(B)). The diameter of these vesicles averaged 270 nm which was the original diameter of the intravenously administered PEG(0.6)-[SA-Ve]. Several similar BMMϕ with vesicles in endosomes and lysosomes were observed, while no vesicles were observed

Table 2
Biodistribution of PEG(0.6)-[SA-Ve] and ^{99m}Tc-HMPAO/glutathione as a percent of the injected dose (%ID) and %ID per gram of tissue at 6 h after i.v. infusion in rabbits

Organs	PEG(0.6)-[SA-Ve]		^{99m}Tc-HMPAO/glutathione	
	%ID ± SEM (%)	%ID/g tissue ± SEM (%/g)	%ID ± SEM (%)	%ID/g tissue ± SEM (%/g)
Blood	6.58 ± 2.91	0.065 ± 0.028	3.34 ± 1.68	0.025 ± 0.013
Bone marrow	69.74 ± 0.86	0.806 ± 0.048	1.13 ± 0.24	0.010 ± 0.001
Liver	11.51 ± 2.88	0.237 ± 0.067	1.52 ± 0.14	0.022 ± 0.001
Spleen	5.00 ± 1.19	5.387 ± 0.807	0.01 ± 0.00	0.011 ± 0.001
Bowel	5.85 ± 0.31	0.014 ± 0.000	4.41 ± 0.19	0.009 ± 0.000
Skin	1.57 ± 0.21	0.009 ± 0.001	2.34 ± 0.30	0.010 ± 0.001
Kidney	2.40 ± 0.10	0.148 ± 0.011	6.11 ± 0.53	0.440 ± 0.066
Muscle	1.86 ± 0.17	0.003 ± 0.000	2.60 ± 0.63	0.002 ± 0.001
Lung	0.19 ± 0.03	0.024 ± 0.006	0.12 ± 0.03	0.010 ± 0.001
Heart	0.03 ± 0.01	0.010 ± 0.002	0.03 ± 0.01	0.006 ± 0.001
Brain	0.01 ± 0.00	0.002 ± 0.000	0.01 ± 0.00	0.001 ± 0.000
Testis	0.03 ± 0.01	0.024 ± 0.005	0.02 ± 0.00	0.008 ± 0.002
Urine	3.57 ± 1.74	—	76.91 ± 4.80	—

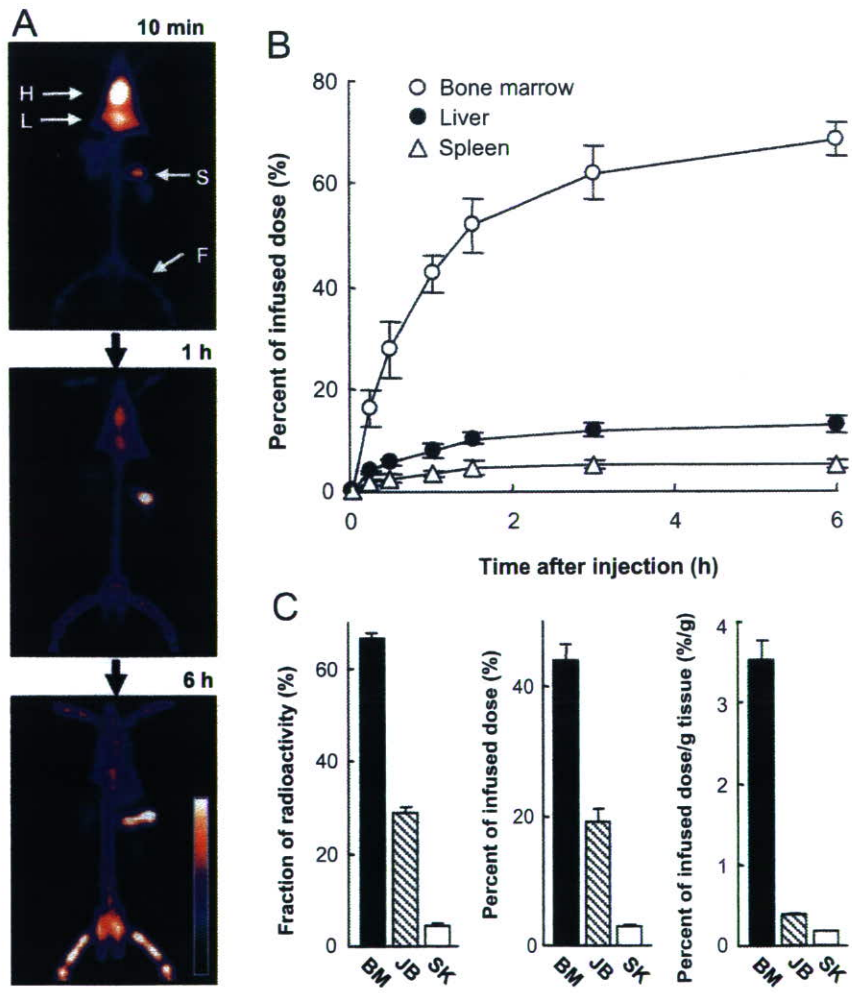

Fig. 3. Initial distribution kinetics of PEG(0.6)-[SA-Ve] after i.v. infusion (lipids: 15 mg/kg b.w.) in rabbits. (A) Gamma camera images of rabbits acquired at various times after infusion. H: heart, L: liver, S: spleen, F: femur. (B) Distribution profiles as a percentage of the injected dose analyzed from the gamma camera images. The total bone marrow was estimated to be 12 times that of one femur. (C) Distribution of radioactivity of PEG(0.6)-[SA-Ve] in separated soft bone marrow (BM), joint bone (sponge bone) (JB), and skeleton (SK) of one femur collected at 6 h after i.v. infusion. Three panels show the fraction of radioactivity, percent of injected dose (%ID), and %ID/g tissue, respectively.

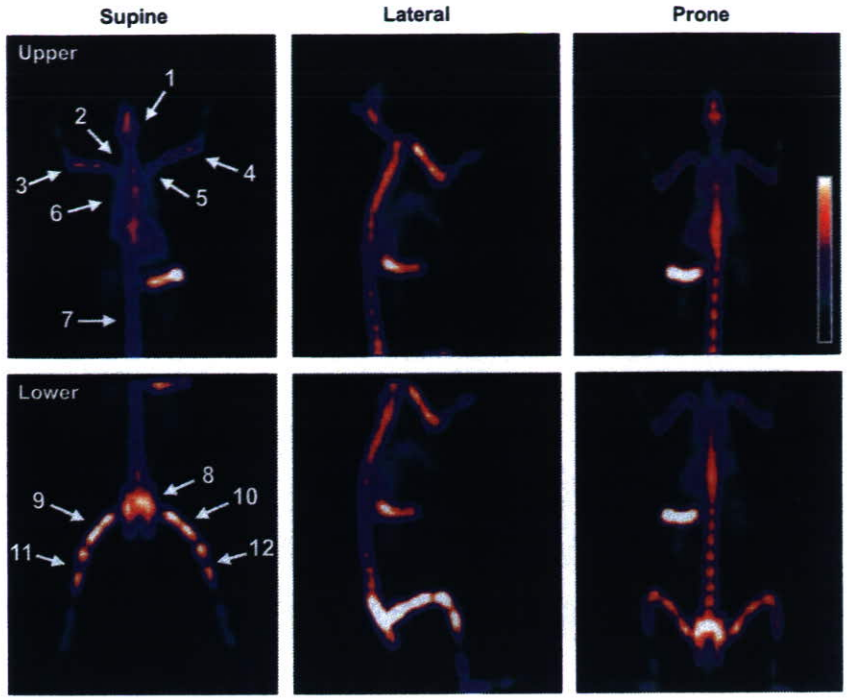

Fig. 4. Gamma camera images of rabbit receiving PEG(0.6)-[SA-Ve], acquired from various angles at 6 h after i.v. infusion. Bone marrow is clearly displayed in these images throughout the rabbit body. Relative radioactivity in separated bone parts were calculated to 1; head (8.41 ± 1.58%), 2; neck (1.10 ± 0.11%), 3; right arm (5.72 ± 0.33%), 4; left arm (5.54 ± 0.40%), 5; shoulder (3.62 ± 0.69%), 6; sternum (4.11 ± 1.35%), 7; spine (21.23 ± 0.42%), 8; pelvis (18.09 ± 0.60%), 9; right femur (7.97 ± 0.05%), 10; left femur (8.34 ± 0.18%), 11; distal right foot (7.88 ± 0.25%), and 12; distal left foot (7.98 ± 0.33%) as percentages to radioactivity of whole bone ± SEM.

in other types of cell such as granular leukocytes, erythroblasts, and endothelial cells in observed section. These microscopic localization studies demonstrate that BMMϕ are the cellular components responsible for clearance of vesicles from the circulation and their uptake by the bone marrow.

4. Discussion

These studies demonstrate that PEG-[SA-Ve] are efficient carriers for targeting the BMMϕ. These vesicles should be useful in the development of bone marrow targeted agents for therapeutic applications. Additionally, this *in vivo* model appears to be an ideal model with which to investigate the role of BMMϕ in the hematopoietic environment. The radiolabeling method for the vesicles encapsulating glutathione with ^{99m}Tc-HMPAO has previously been established for imaging studies [14,23,24]. In the present vesicle formulation, we confirmed the stability of the ^{99m}Tc radiolabeled-vesicles during incubation in serum and plasma at 37 °C for 48 h (more than 95% remaining with vesicles), and we also determined that the free labeling agent is not specifically distributed into organs such as bone marrow, liver, and spleen, but rapidly eliminated through renal excretion as shown in Fig. 2 and Table 2. This evidence provides strong support that the radioisotope distribution reflects the true biodistribution of vesicles. As shown in Fig. 1, comparative data showing the organ distribution of several formulations clearly demonstrated that the uptake of vesicles by bone marrow is induced by the incorporation of SA ($p < 0.01$); furthermore, the incorporation of a small amount of PEG-DSPE on the surface of SA-Ve prolongs its circulation time and tends to enhance the bone marrow selectivity by preventing hepatic uptake. Thus, maximum distribution to bone marrow was observed at 0.6 mol% PEG-DSPE (Fig. 1(B)). The degree of hepatic uptake was reduced as the PEG-DSPE content increased, and this effect became significant above 1.4 mol% ($p < 0.05$). Bone marrow uptake was also reduced above 1.4 mol%. In general, 5–10 mol% of PEG-lipids is incorporated into most of the long circulating vesicle formulations for passive targeting [8,9]. In the present study, prolonged circulation time of vesicles was observed above 0.6 mol% of PEG-DSPE, and the circulation times were prolonged more in vesicles with higher PEG-DSPE content. For the effective targeting of bone marrow, however, higher concentrations of PEG blocked the active targeting of the vesicles to bone marrow. These results indicate that the dense PEG layer on the vesicular surface covers the surface properties having the character of SA and depress uptake by BMMϕ. Therefore, the optimal amount of PEG incorporation was found to be 0.6 mol%, as this concentration passively enhances active targeting. Theoretically, approximately 0.4 mol% of PEG (Mw 5000)-lipids is estimated to be the critical content required to fully cover the vesicle surface which consists of DPPC and CH (1:1 molar ratio) with the mushroom conformation of PEG chains from Eqs. (1) to (3). Thus, it is

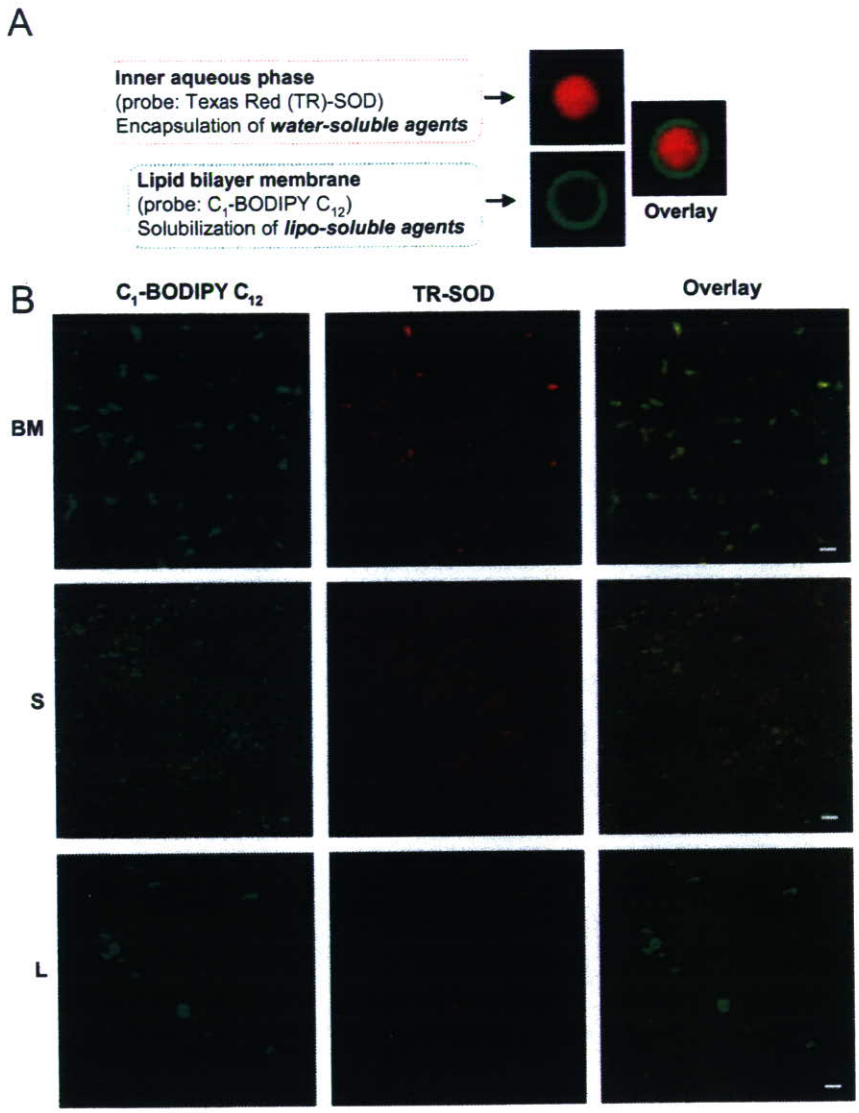

Fig. 5. Histological examination of fluorescence delivered into bone marrow tissues using PEG(0.6)-[SA-Ve] as carriers. (A) Fluorescence localization in double fluorescence-labeled large multilamellar PEG(0.6)-[SA-Ve] with diameter of ca. 10 μm. This observation was performed before extrusion to submicron size to enable observation of the structure within resolution of a confocal microscope. This image indicates that red fluorescence comes from TR-SOD which is encapsulated in inner aqueous phase and green fluorescence comes from C_1-BODIPY C_{12} which is embedded in bilayer membrane. (B) Confocal scanning images of femoral bone marrow (BM), spleen (S), and liver (L) taken from rabbit at 6 h after i.v. injection of double fluorescence-labeled PEG(0.6)-[SA-Ve] with size of 247 ± 22 nm in diameter (lipids: 15 mg/kg b.w.). The scale bars represent 20 μm.

estimated that the optimal incorporation amount of PEG-lipids is slightly higher than that required to fully cover the vesicular surface. This finding provides useful information for the design of vesicle surface to passively enhance the active targeting with PEG-modification *in vivo*.

To examine the participation of the anionic properties of vesicles in BMMϕ uptake, we investigated the organ distribution of conventional anionic vesicles containing PG with same protocol. These PG-vesicles do not distribute to the bone marrow (Supplementary Table 2 online, only 5.36 ± 0.65%ID of PG-vesicles were taken up by the bone marrow at 24 h after i.v. injection). Comparative data for Ve and SA-Ve are shown in Fig. 1(B) and Supplementary Table 1. Previous publications have also supported the observation that PG-vesicles do not distribute to the bone marrow [33], and neutral vesicles with various sizes in the range of 136.2–318 nm do not distribute to the bone marrow [34]. These results indicated that the targeting of bone marrow is not general for neutral vesicles and is achieved not only by the anionic surface of vesicles. The results suggest that SA is specifically responsible for the bone marrow targeting.

Histological observations showed that the vesicles and encapsulated agents are distributed at the same locations into bone marrow tissues, clearly indicating that the encapsulated agents were delivered to the bone marrow tissues by the vesicles (Fig. 5). Higher magnification TEM observations have demonstrated that a massive number of vesicles are trapped in the endosomes and lysosomes of the BMMϕ (Fig. 6). These observations indicated that the

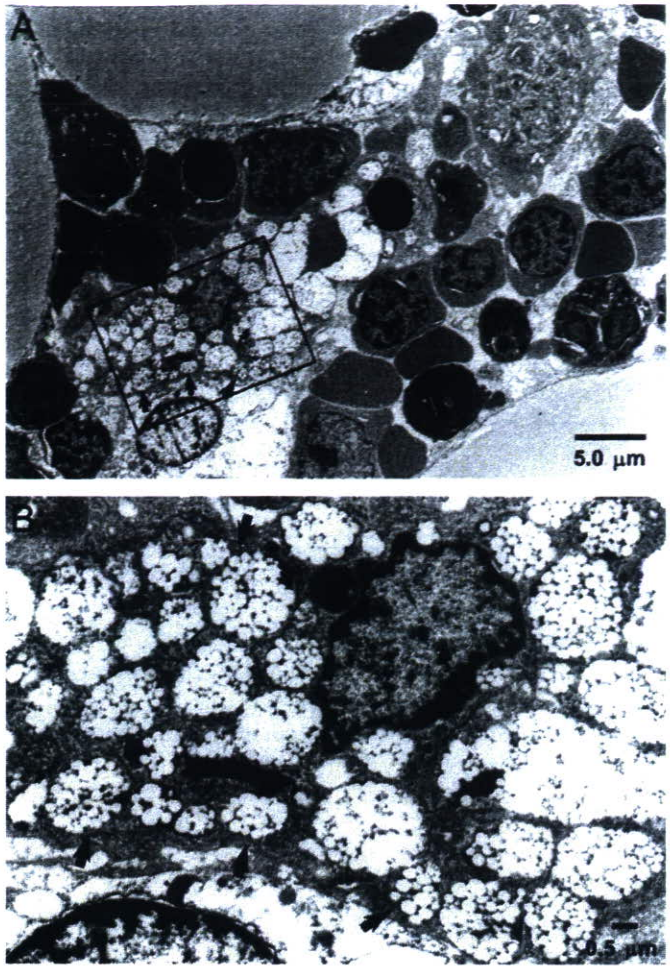

Fig. 6. Transmission electron micrographs of femoral bone marrow tissue section, taken from rabbit at 6 h after i.v. injection of PEG(0.6)-[SA-Ve] (lipids: 15 mg/kg b.w.). (A) Low magnified micrograph representing the bone marrow tissue including macrophage and various bone marrow cells. (B) High magnified micrograph of framed region in panel (A). A massive number of vesicles with original diameter (average 270 nm) are trapped in several endosomes or lysosomes of macrophage. Some are indicated by arrows, which shows same position in (A) and (B).

uptake of PEG(0.6)-[SA-Ve] by bone marrow was responded by the endocytosis of BMMϕ. One potent trigger to accelerate the cellular endocytosis for vesicles is an interaction with the receptors on the surface of cells, that are known as a receptor-mediated endocytosis which is investigated as a potent pathway for drug targeting to specific cell including macrophage [2,10,11]. Scavenger receptors are membrane glycoproteins that are present mainly on cells of the macrophage lineage [35,36]. Various polyanionic compounds such as dextran sulfate, polyinosinic acid, and acetylated low density lipoproteins have been reported as ligands for this receptor [37,38]. These compounds are taken at high levels by macrophages via a scavenger receptor-mediated mechanism. On the other hand, many polyanions such as chondroitin sulfate, poly(D-glutamic) acid, and polycytidylic acid are not ligands for scavenger receptors [37,38]. Previous investigations indicated that the scavenger receptors on macrophages contribute to the recognition of polyanionic structures, resulting in selective uptake. Enhanced uptake of succinylated proteins has been investigated in cultured brain microvessel endothelial cells. Endothelial cells also express the scavenger receptor on their surface. Large succinylated proteins such as catalase (Mw 227 kDa) and bovine serum albumin (Mw 70 kDa) were taken up by the cells via a scavenger receptor-mediated mechanism, whereas significant uptake was not observed for native proteins and small succinylated proteins such as SOD (Mw 34 kDa) and soybean trypsin inhibitor (Mw 21 kDa) [39]. This indicates that succinylation of large molecules is involved in the uptake via a scavenger receptor-mediated mechanism. Recently, Szabó et al. reported the uptake of branched polypeptides by bone marrow culture-derived murine macrophages. They indicated that the succinylation of branched polypeptides significantly enhanced the uptake by macrophages, and the uptake was inhibited by blocking of the class-A scavenger receptors [40]. Because the terminal hydrophilic head group of SA is corresponding to the succinylated structure, we speculate that the interaction between PEG-[SA-Ve] and the scavenger receptors on BMMϕ might participate in the selective uptake. However, further mechanistic investigation on uptake of PEG-[SA-Ve] by BMMϕ, splenic macrophages, and hepatic Kupffer cells is necessary to clarify the mechanism of organ selective macrophage uptake.

Previous pharmacokinetic studies have been performed using vesicles containing SA that have the same lipid composition as in the present study with PEG(0.3)-[SA-Ve], but a significantly higher dose was employed (lipids: 680 mg/kg b.w.) [17]. In these studies, the bone marrow-selective distribution was not observed, so it appears that the bone marrow selectivity is limited by the injection dosage in certain applications. As the vesicle dosage increases, the MPS in the bone marrow becomes saturated; as a result, liver and spleen uptake is increased. In our previous organ distribution study in rabbits, $>50\%$ID of the vesicles were still in circulation at 48 h after infusion of a massive dose of vesicles, while the bone marrow had $7.36 \pm 0.34\%$ of 680 mg/kg b.w. at the same time point [17]. This value is equivalent to 50.0 mg/kg b.w., and it can be used to estimate the maximum uptake capacity of MPS for vesicles. When vesicle dosage increases above 50.0 mg/kg b.w., the bone marrow is the first organ to become saturated, and the accumulation of vesicles then increases in the liver and spleen. Such sequential saturation of the MPS eliminates organ selectivity. Therefore, the bone marrow targeting of SA-Ve becomes striking when the dose of vesicles is below the saturation dosage for bone marrow, as observed in the present study (15 mg/kg b.w.). The ability of vesicular nanoparticles to encapsulate a wide variety of agents provides significant opportunities for bone marrow delivery applications. In the present study, we have demonstrated the delivery of scintigraphic and fluorescence imaging agents to bone marrow by using the

SA-Ve vesicles. This method has advantages in delivering the therapeutic agents to treat bone marrow disorders.

5. Conclusion

This is the first report to show the organ distribution of PEG-[SA-Ve] at small dose injection. Organ distributions of several vesicular formulations were quantitatively compared to determine the component to induce the significant distribution into bone marrow. Our data have indicated that surface modification of phospholipid vesicles with two compounds, SA and PEG-DSPE, cooperatively induces the significant bone marrow targeting properties to vesicles. In this system, BMMϕ participated in the uptake of PEG-[SA-Ve], and the efficient delivery of the vesicles as encapsulating agents into the bone marrow was achieved within 6 h after injection. These results indicated that the PEG-[SA-Ve] is a potent carrier for drug delivery into BMMϕ *in vivo* and may be useful for delivering a wide range of therapeutic agents to bone marrow.

Acknowledgments

This work was partly supported by project of a Health and Labor Sciences Research Grant (Research on Pharmaceutical and Medical Safety, Artificial Blood Project) of the Ministry of Health, Labor and Welfare, Japan, and the Ministry of Education, Culture, Sports, Science and Technology, Grant-in-Aid for Scientific Research (B), 17300162, 2005. The authors gratefully acknowledge Dr. H. Sakai (Waseda University) for discussions on this research, Dr. Linda M. McManus (UTHSCSA) for assistance with electron microscopic images and Mr. R. Klipper (UTHSCSA) for technical support.

Appendix A. Supplementary materials

The online version of this article contains additional supplementary data. Please visit doi:10.1016/j.biomaterials.2007.01.041.

References

[1] Farokhzad OD, Jon S, Khademhosseini A, Tran TN, Lavan DA, Langer R. Nanoparticle–aptamer bioconjugates: a new approach for targeting prostate cancer cells. Cancer Res 2004;64:7668–72.
[2] Torchilin VP. Recent advances with liposomes as pharmaceutical carriers. Nat Rev Drug Discov 2005;4:145–60.
[3] Gregoriadis G, Wills EJ, Swain CP, Tavill AS. Drug-carrier potential of liposomes in cancer chemotherapy. Lancet 1974;1:1313–6.
[4] Felgner PL, Gadek TR, Holm M, Roman R, Chan HW, Wenz M, et al. Lipofection: a highly efficient, lipid-mediated DNA-transfection procedure. Proc Natl Acad Sci USA 1987;84:7413–7.
[5] Moghimi SM, Hunter AC, Murray JC. Long-circulating and target-specificity nanoparticles: theory to practice. Pharmacol Rev 2001;53:283–318.
[6] Sakai H, Horinouchi H, Tomiyama K, Ikeda E, Takeoka S, Kobayashi K, et al. Hemoglobin-vesicles as oxygen carriers: influence on phagocytic activity and histopathological changes in reticuloendothelial system. Am J Pathol 2001;159:1079–88.
[7] Fadok VA, Bratton DL, Rose DM, Pearson A, Ezekewitz RA, Henson PM. A receptor for phosphatidylserine-specific clearance of apoptotic cells. Nature 2000;405:85–90.
[8] Klibanov AL, Maruyama K, Torchilin VP, Huang L. Amphipathic polyethyleneglycols effectively prolong the circulation time of liposomes. FEBS Lett 1990;268:235–7.
[9] Gabizon A, Shmeeda H, Barenholz B. Pharmacokinetics of pegylated liposomal Doxorubicin: review of animal and human studies. Clin Pharmacokinet 2003;42:419–36.
[10] Turk MJ, Water DJ, Low PS. Folate-conjugated liposomes preferentially target macrophages associated with ovarian carcinoma macrophage. Cancer Lett 2004;213:165–72.
[11] Chellat F, Merhi Y, Moreau A, Yahia L'H. Therapeutic potential of nanoparticulate systems for macrophage targeting. Biomaterials 2005;26:7260–75.
[12] Mantovani A, Sozzani S, Locati M, Allavena P, Sica A. Macrophage polarization: tumor-associated macrophages as a paradigm for polarized M2 mononuclear phagocytes. Trends Immunol 2002;23:549–55.
[13] Allen TM, Austin GA, Chonn A, Lin L, Lee KC. Uptake of liposomes by cultured mouse bone marrow macrophages: influence of liposome composition and size. Biochim Biophys Acta 1991; 1061:56–64.
[14] Phillips WT, Klipper RW, Awasthi VD, Rudolph AS, Cliff R, Kwasiborski V, et al. Polyethylene glycol-modified liposome-encapsulated hemoglobin: a long circulating red cell substitute. J Pharmacol Exp Ther 1999;288:665–70.
[15] Dams ET, Oyen WJ, Boerman OC, Storm G, Laverman P, Kok PJ, et al. ^{99m}Tc-PEG liposomes for the scintigraphic detection of infection and inflammation: clinical evaluation. J Nucl Med 2000;41:622–30.
[16] Giuliani AL, Wiener E, Lee MJ, Brown IN, Berti G, Wickramasinghe SN. Changes in murine bone marrow macrophages and erythroid burst-forming cells following the intravenous injection of liposome-encapsulated dichloromethylene diphosphonate (Cl_2MDP). Eur J Haematol 2001;66:221–9.
[17] Sou K, Klipper R, Goins B, Tsuchida E, Phillips WT. Circulation kinetics and organ distribution of Hb-vesicles developed as a red blood cell substitute. J Pharmacol Exp Ther 2005; 312:702–9.
[18] Sadahira Y, Mori M. Role of the macrophage in erythropoiesis. Pathol Int 1999;49:841–8.
[19] Yoshida H, Kawane K, Koike M, Mori Y, Uchiyama Y, Nagata S. Phosphatidylserine-dependent engulfment by macrophages of nuclei from erythroid precursor cells. Nature 2005;437:754–8.
[20] Sou K, Naito Y, Endo T, Takeoka S, Tsuchida E. Effective encapsulation of proteins into size-controlled phospholipid vesicles using freeze–thawing and extrusion. Biotechnol Prog 2003;19:1547–52.
[21] Sou K, Endo T, Takeoka S, Tsuchida E. Poly(ethylene glycol)-modification of the phospholipid vesicles by using the spontaneous incorporation of poly(ethylene glycol)-lipid into the vesicles. Bioconjug Chem 2000;11:372–9.
[22] Sakai H, Hisamoto S, Fukutomi I, Sou K, Takeoka S, Tsuchida E. Detection of lipopolysaccharide in hemoglobin-vesicles by Limulus amebocyte lysate test with kinetic-turbidimetric gel clotting analysis and pretreatment of surfactant. J Pharm Sci 2004;93: 310–21.
[23] Rudolph AS, Klipper R, Goins B, Phillips WT. *In vivo* biodistribution of a radiolabeled blood substitute: ^{99m}Tc-labeled liposome-encapsulated hemoglobin in an anesthetized rabbit. Proc Natl Acad Sci USA 1991;88:10976–80.
[24] Phillips WT, Rudolph AS, Goins B, Timmons JH, Klipper R, Blumhardt R. A simple method for producing a technetium-99m-labeled liposome which is stable *in vivo*. Nucl Med Biol 1992;19:539–47.

[25] Awasthi V, Goins B, Klipper R, Loredo R, Korvick D, Phillips WT. Dual radiolabeled liposomes: biodistribution studies and localization of focal sites of infection in rats. Nucl Med Biol 1998;25:155–60.
[26] Kozma C, Macklin W, Cummins LM, Mauer R. Anatomy, physiology, and biochemistry of the rabbit. In: Weisbroth SH, Flatt RE, Kraus AL, editors. The biology of the laboratory rabbit. New York: Academic Press; 1974. p. 50–69.
[27] Kaplan HM, Timmons EH. The rabbit: a model for the principles of mammalian physiology and surgery. New York: Academic Press; 1979.
[28] Deitz AA. Distribution of bone marrow, bone and bone ash in rabbits. Proc Soc Exp Med 1944;57:60–2.
[29] Lefevre C, Kang HC, Haugland RP, Malekzadeh N, Arttamangkul S, Haugland RP. Texas Red-X and rhodamine Red-X, new derivatives of sulforhodamine 101 and lissamine rhodamine B with improved labeling and fluorescence properties. Bioconjug Chem 1996;7:482–9.
[30] Torchilin VP, Papisov MI. Why do polyethylene glycol-coated liposomes circulate so long? J Liposome Res 1994;4:725–39.
[31] Du H, Chandaroy P, Hui SW. Grafted poly-(ethylene glycol) on lipid surface inhibits protein adsorption and cell adhesion. Biochim Biophys Acta 1997;1326:236–48.
[32] Edholm O, Nagle JF. Areas of molecules in membranes consisting mixtures. Biophys J 2005;89:1827–32.
[33] Awasthi VD, Garcia D, Klipper R, Goins BA, Phillips WT. Neutral and anionic liposome-encapsulated hemoglobin: effect of postinserted poly(ethylene glycol)-distearoylphosphatidylethanolamine on distribution and circulation kinetics. J Pharmacol Exp Ther 2004; 309:241–8.
[34] Awasthi VD, Garcia D, Goins BA, Phillips WT. Circulation and biodistribution profiles of long-circulating PEG-liposomes of various sizes in rabbits. Int J Pharm 2003;253:121–32.
[35] Doi T, Higashino K, Kurihara Y, Wada Y, Miyazaki T, Nakamura H, et al. Charged collagen structure mediates the recognition of negatively charged macromolecules by macrophage scavenger receptors. J Biol Chem 1993;268:2126–33.
[36] Taylor PR, Martinez-Pomares L, Stacey M, Lin HH, Brown GD, Gordon S. Macrophage receptors and immune recognition. Annu Rev Immunol 2005;23:901–44.
[37] Brown MS, Goldstein JL. Lipoprotein metabolism in the macrophage: implications for cholesterol deposition in atherosclerosis. Annu Rev Biochem 1983;52:223–61.
[38] Krieger M, Acton S, Ashkenas J, Pearson A, Penman M, Resnick D. Molecular flypaper, host defense, and atherosclerosis. Structure, binding properties, and functions of macrophage scavenger receptors. J Biol Chem 1993;268:4569–72.
[39] Tokuda H, Masuda S, Takakura Y, Sezaki H, Hashida M. Specific uptake of succinylated proteins via a scavenger receptor-mediated mechanism in cultured brain microvessel endothelial cells. Biochem Biophys Res Commun 1993;196:18–24.
[40] Szabó R, Peiser L, Plüddemann A, Bösze S, Heinsbroek S, Gordon S, et al. Uptake of branched polypeptides with poly[L-lys] backbone by bone-marrow culture-derived murine macrophages: the role of the class a scavenger receptor. Bioconjug Chem 2005;16:1442–50.